Research Article | Vol. 25, No. 26 | 25 Dec 2017 | OPTICS EXPRESS 32227
Optics EXPRESS

Generation of highly pure Schrödinger's cat states and real-time quadrature measurements via optical filtering

WARIT ASAVANANT,[1,3] KOTA NAKASHIMA,[1] YU SHIOZAWA,[1] JUN-ICHI YOSHIKAWA,[1,2] AND AKIRA FURUSAWA[1,4]

[1] *Department of Applied Physics, School of Engineering, The University of Tokyo, 7-3-1 Hongo, Bunkyo-ku, Tokyo, 113-8656, Japan*
[2] *Quantum-Phase Electronics Center, School of Engineering, The University of Tokyo, 7-3-1 Hongo, Bunkyo-ku, Tokyo, 113-8656, Japan*
[3] *warit@alice.t.u-tokyo.ac.jp*
[4] *akiraf@ap.t.u-tokyo.ac.jp*

Abstract: In the generation of Schrödinger's cat states using an optical parametric oscillator in the continuous-wave regime up until now, single photons are subtracted from the whole bandwidth of the squeezed vacua. However, it was pointed out recently that the achievable purities are limited in such method [J. Yoshikawa, W. Asavanant, and A. Furusawa, Phys. Rev. A **96**, 052304 (2017)]. In this paper, we used our new photon subtraction method with a narrowband filtering cavity and generated a highly pure Schrödinger's cat state with the value of -0.184 ± 0.001 at the origin of the Wigner function. To our knowledge, this is the highest value ever reported without any loss corrections. The temporal mode also becomes exponentially rising in our method, which we utilize to make a real-time quadrature measurement on Schrödinger's cat states, and we obtained the value of -0.162 ± 0.001 at the origin of the Wigner function.

OCIS codes: (270.0270) Quantum optics; (270.5585) Quantum information and processing; (270.6570) Squeezed states.

References and links

1. H. Jeong and M. S. Kim, "Efficient Quantum Computation using Coherent States," Phys. Rev. A **65**, 042305 (2002).
2. T. Ralph, A. Gilchrist, G. J. Milburn, W. J. Munro, and S. Glancy, "Quantum computation with optical coherent states," Phys. Rev. A **68**, 042319 (2003).
3. A. P. Lund, T. C. Ralph, and H. L. Haselgrove, "Fault-tolerant linear optical quantum computing with small-amplitude coherent states," Phys. Rev. Lett. **100**, 030503 (2008).
4. J. S. Neergaard-Nielsen, M. Takeuchi, K. Wakui, H. Takahashi, K. Hayasaka, M. Takeoka, and M. Sasaki, "Optical continuous-variable qubit," Phys. Rev. Lett. **105**, 053602 (2010).
5. V. Karimipour, A. Bahraminasab, and S. Bagherinezhad, "Entanglement swapping of generalized cat states and secret sharing," Phys. Rev. A **65**, 042320 (2002).
6. J. B. Brask, I. Rigas, E. S. Polzik, U. L. Andersen, and A. S. Sørensen, "Hybrid long-distance entanglement distribution protocol," Phys. Rev. Lett. **105**, 160501 (2010).
7. N. Sangouard, C. Simon, N. Gisin, J. Laurat, R. Tualle-Brouri, and P. Grangier, "Quantum repeaters with entangled coherent states," J. Opt. Soc. Am. B **27**, A137–A145 (2010).
8. A. Gilchrist, K. Nemoto, W. J. Munro, T. C. Ralph, S. Glancy, S. L. Braunstein, and G. J. Milburn, "Schrödinger cats and their power for quantum information processing," J. Opt. B: Quantum Semiclassical Opt. **6**, S828–S833 (2004).
9. D. Gottesman and I. L. Chuang, "Demonstrating the viability of universal quantum computation using teleportation and single-qubit operations," Nature **402**, 390–393 (1999).
10. R. Raussendorf and H. J. Briegel, "A One-Way Quantum Computer," Phys. Rev. Lett. **86**, 5188 (2001).
11. B. Yurke and D. Stoler, "Generating quantum mechanical superpositions of macroscopically distinguishable states via amplitude dispersion," Phys. Rev. Lett. **57**, 13 (1986).
12. M. Dakna, T. Anhut, T. Opatrný, L. Knöll, and D.-G. Welsch, "Generating Schrödinger-cat-like states by means of conditional measurements on a beam splitter," Phys. Rev. A **55**, 3184 (1997).
13. A. P. Lund, H. Jeong, T. C. Ralph, and M. S. Kim, "Conditional production of superpositions of coherent states with inefficient photon detection," Phys. Rev. A **70**, 020101 (2004).
14. A. Ourjoumtsev, R. Tualle-Brouri, J. Laurat, and P. Grangier, "Generating Optical Schrodinger Kittens for Quantum Information Processing," Science **312**, 83–86 (2006).
15. J. S. Neergaard-Nielsen, B. M. Nielsen, C. Hettich, K. Mølmer, and E. S. Polzik, "Generation of a superposition of odd photon number states for quantum information networks," Phys. Rev. Lett. **97**, 083604 (2006).

#304868 https://doi.org/10.1364/OE.25.032227
Journal © 2017 Received 15 Aug 2017; revised 19 Oct 2017; accepted 28 Nov 2017; published 11 Dec 2017

Optics EXPRESS

16. K. Wakui, H. Takahashi, A. Furusawa, and M. Sasaki, "Photon subtracted squeezed states generated with periodically poled KTiOPO(4)," Opt. Express **15**, 3568–3574 (2007).
17. H. Takahashi, K. Wakui, S. Suzuki, M. Takeoka, K. Hayasaka, A. Furusawa, and M. Sasaki, "Generation of large-amplitude coherent-state superposition via ancilla-assisted photon subtraction," Phys. Rev. Lett. **101**, 233605 (2008).
18. T. Gerrits, S. Glancy, T. S. Clement, B. Calkins, A. E. Lita, A. J. Miller, A. L. Migdall, S. W. Nam, R. P. Mirin, and E. Knill, "Generation of optical coherent-state superpositions by number-resolved photon subtraction from the squeezed vacuum," Phys. Rev. A **82**, 031802 (2010).
19. O. Morin, K. Huang, J. Liu, H. Le Jeannic, C. Fabre, and J. Laurat, "Remote creation of hybrid entanglement between particle-like and wave-like optical qubits," Nat. Photonics **8**, 570 (2014).
20. J. Etesse, M. Bouillard, B. Kanseri, and R. Tualle-Brouri, "Experimental generation of squeezed cat states with an operation allowing iterative growth," Phys. Rev. Lett. **114**, 193602 (2015).
21. K. Huang, H. Le Jeannic, J. Ruaudel, V. B. Verna, M. D. Shaw, F. Marsili, S. W. Nam, E Wu, H. Zeng, Y. -C. Jeong, R. Filip, O. Morin, and J. Laurat, "Optical synthesis of large-amplitude squeezed coherent-state superpositions with minimal resources," Phys. Rev. Lett. **115**, 023602 (2015).
22. D. V. Sychev, A. E. Ulanov, A. A. Pushkina, M. W. Richards, I. A. Fedorov, and A. I. Lvovsky, "Enlargement of optical Schrödinger's cat states," Nat. Photonics **11**, 379–382 (2017).
23. J. Yoshikawa, W. Asavanant, and A. Furusawa, "Purification of photon subtraction from continuous squeezed light by filtering," Phys. Rev. A **96**, 052304 (2017).
24. M. Gu, C. Weedbrook, N. C. Menicucci, T. C. Ralph, P. van Loock, "Quantum computing with continuous-variable clusters," Phys. Rev. A **79**, 062318 (2009).
25. K. Miyata, H. Ogawa, P. Marek, R. Filip, H. Yonezawa, J. Yoshikawa, and A. Furusawa, "Implementation of a quantum cubic gate by an adaptive non-Gaussian measurement," Phys. Rev. A **93**, 022301 (2016).
26. S. D. Bartlett, B. C. Sanders, S. L. Braunstein, and K. Nemoto, "Efficient classical simulation of continuous variable quantum information processes," Phys. Rev. Lett. **88**, 097904 (2002).
27. D. Gottesman, A. Kitaev, and J. Preskill, "Encoding a qubit in an oscillator," Phys. Rev. A **64**, 012310 (2001).
28. H. Ogawa, H. Ohdan, K. Miyata, M. Taguchi, K. Makino, H. Yonezawa, J. Yoshikawa, and A. Furusawa, "Real-Time Quadrature Measurement of a Single-Photon Wave Packet with Continuous Temporal-Mode Matching," Phys. Rev. Lett. **116**, 233602 (2016).
29. Z. Qin, A. S. Prasad, T. Brannan, A. MacRae, A. Lezama, and A. Lvovsky, "Complete temporal characterization of a single photon," Light Sci. Appl. **4**, e298 (2015).
30. B. Srivathsan, G. K. Gulati, A. Cerè, B. Chng, and C. Kurtsiefer, "Reversing the temporal envelope of a heralded single photon using a cavity," Phys. Rev. Lett. **113**, 163601 (2014).
31. N. Lee, H. Benichi, Y. Takeno, S. Takeda, J. Webb, E. Huntington, and A. Furusawa, "Teleportation of nonclassical wave packets of light," Science **332**, 330–333 (2011).
32. T. Serikawa, J. Yoshikawa, K. Makino, and A. Furusawa, "Creation and Measurement of Broadband Squeezed Vacuum from a Ring Optical Parametric Oscillator," Opt. Express **24**, 28383–28391 (2016).
33. R. W. P. Drever, J. L. Hall, F. V. Kowalski, J. Hough, G. M. Ford, A. J. Munley, and H. Ward, "Laser Phase and Frequency Stabilization Using an Optical Resonator," Appl. Phys. B **31**, 97–105 (1983).
34. D. A. Shaddock, M. B. Gray, and D. E. McClelland, "Frequency locking a laser to an optical cavity by use of spatial mode interference," Opt. Lett. **24**, 1499–1501 (1999).
35. K. Mølmer, "Non-Gaussian states from continuous-wave Gaussian light sources," Phys. Rev. A **73**, 063804 (2006).
36. A. I. Lvovsky, "Iterative maximum-likelihood reconstruction in quantum homodyne tomography," J. Opt. B: Quantum Semiclassical Opt. **6**, S556-S559 (2004).
37. A. I. Lvovsky and M. G. Raymer, "Continuous-variable optical quantum-state tomography," Rev. Mod. Phys. **81**, 299 (2009).
38. M. J. Collett, and C. W. Gardiner, "Squeezing of intracavity and traveling-wave light fields produced in parametric amplification," Phys. Rev. A **30**, 1386 (1984).
39. P. Comon, "Independent component analysis, A new concept?" Signal Processing **36**, 287–314 (1994).
40. A. MacRae, T. Brannan, R. Achal, and A. I. Lvovsky, "Tomography of a High-Purity Narrowband Photon from a Transient Atomic Collective Excitation," Phys. Rev. Lett. **109**, 033601 (2012).
41. O. Morin, C. Fabre, and J. Laurat, "Experimentally accessing the optimal temporal mode of traveling quantum light states," Phys. Rev. Lett. **111**, 213602 (2013).
42. B. Efron and R. Tibshirani, *An introduction to the bootstrap* (Chapman & Hall, 1993).

1. Introduction

Generation of highly nonclassical states with high purity and fidelity is challenging but necessary for quantum information processing. One of the states with such high nonclassicality is a quantum superposition of macroscopically distinguishable states; so-called Schrödinger's cat states with the name taken from the famous Schrödinger's cat paradox. The optical Schrödinger's cat states

Optics EXPRESS

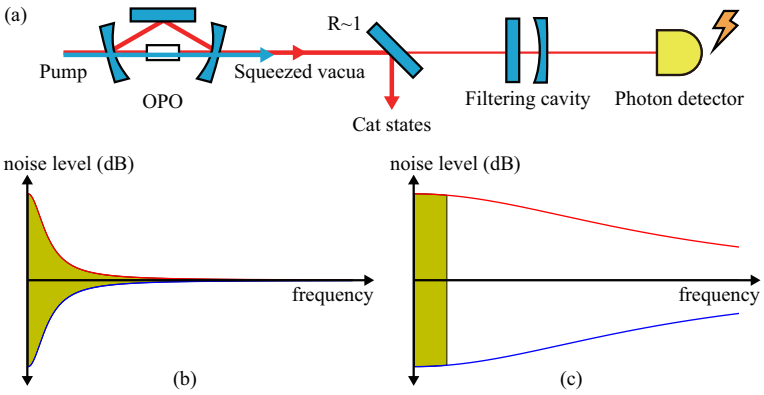

Fig. 1. Schematic diagram of photon subtraction and comparison of relation of squeezed spectra and frequency bandwidth of subtracted photon between previous demonstrations and our optical filtering method. (a) Schematic diagram of photon subtraction. (b) Previous demonstrations. (c) our method. Red line: anti-squeezing level. Blue line: squeezing level. Area painted with yellow: frequency bandwidth of photon subtracted from squeezed state.

refer to the superposition of coherent states: $|\alpha\rangle + e^{i\theta}|-\alpha\rangle$, where $|\alpha\rangle$ is a coherent state with complex amplitude α. Cat states do not only pose an interest in fundamental quantum physics, but also possess many potential applications, such as quantum computation [1–4], entanglement distribution and quantum key distribution [5–7], and quantum metrology [8]. In optical continuous-varible (CV) quantum information processing, the measurement-based quantum computation (MBQC) is currently the most promising method in terms of operation implementation and scalability [9, 10]. Therefore, the generation of high fidelity and large amplitude α cat states and the combination of such states with MBQC will take us a step closer to the realization of CV optical quantum computing.

The first proposition for the generation of cat states was via the Kerr effect in a nonlinear medium [11]. However, the Kerr effect is usually weak. Instead, the generation by photon subtraction [12, 13] is widely used due to its simplicity in the implementation. In photon subtraction, a single photon is tapped from a squeezed vacuum, and the generated state is heralded by the detection of subtracted single photon (Fig. 1(a)). The cat states generated by this method are usually limited to the case where the amplitude is small, i.e. $|\alpha|^2 \approx 1$. The generation of cat states using photon subtraction has already been demonstrated in both pulsed regime [14] and continuous-wave (CW) regime [15, 16]. Two photons subtraction [17] and three photons subtraction [18] have also been experimentally demonstrated. Moreover, more complex quantum states, such as parity qubits based on cat states [4] and entanglement between single-rail qubits and cat states [19] have also been generated by methods which involve photon subtraction. Regarding the size of the cat states, many progresses have been made in the generation of cat states with large amplitude [20–22].

However, in the recent work by Yoshikawa *et al.* [23], it was shown that the frequency bandwidth of the subtracted photons, which has not been given much attention, affects the purity of the generated cat states. In the previous demonstrations of generation of cat states in CW regime [15, 16], the squeezed vacua are generated from an optical parametric oscillator (OPO), and the whole frequency bandwidth of the squeezed vacua is used in the photon subtraction (Fig. 1(b)). In such method, the achievable purities are limited by the inherent impurities of the initial squeezed vacua. This is due to the fact that when the cat states are heralded by the detection of subtracted single photons, the heralded states exist in a wave packet. In the frequency domain,

Optics EXPRESS

the squeezed vacuum is pure for all frequency. However, when we consider a squeezed state in a wave packet in the time domain, the squeezed vacua become impure, and this impurity affects the subsequently generated cat states. Also, the inherent impurity in squeezing level due to the shape of the wave packets limits the squeezing level before the photon subtraction. In previous photon subtraction, where the temporal mode is double-side exponential, such impurity is calculated to be equivalent to 10% loss [23]. Therefore, roughly speaking, the previous photon subtraction can be performed on squeezing vauca with squeezing level of at most about 10 dB. On the other hand, our method does not have such limitation.

In an ideal photon subtraction from an ideal single-mode-squeezed vacuum, single-mode-squeezed single photon is generated, i.e. $\hat{a}\hat{S}|0\rangle \propto \hat{S}\hat{a}^\dagger|0\rangle$, where $\hat{a}$, $\hat{a}^\dagger$, and $\hat{S}$ are annihilation operator, creation operator, and squeezing operator for single mode, respectively. On the other hand, in photon subtractions from squeezed vacua generated by OPO in CW regime, the generated states are in a wave packet mode and is equivalent to multi-mode-squeezed single photon [23], i.e. $\hat{a}(t)\hat{S}_{\text{multi}}|0\rangle \propto \hat{S}_{\text{multi}}\hat{a}_r^\dagger|0\rangle$, where $\hat{a}(t)$, $\hat{S}_{\text{multi}}$, and $\hat{a}_r^\dagger$ are instantaneous annihilation operator, multi-mode squeezing operator, and creation operator of photon in a temporal mode defined by time correlation of OPO, respectively. The squeezing operation on this single photon can be decomposed into generation of photon pairs in the same mode with $\hat{a}_r^\dagger$ (single-mode-squeezing) and generation of photon pairs where one photon is in the same mode as $\hat{a}_r$ and the other photon is in an orthogonal mode (two-mode-squeezing) [23]. The mode mismatch between the squeezing operator and the temporal mode of $\hat{a}_r^\dagger$ is 10%. In the case of weak pump, this 10% impurity corresponds to single-mode-squeezing and two-mode-squeezing with bias of 3 : 4 [23]. As an estimation, let us consider the cat state generated by photon subtraction from 3 dB squeezed vacuum. In the ideal single-mode-squeezing case, this state has at most around three photons and the ratio of single photon, two photons and three photons component are approximately 85%, 0%, and 15%, respectively. In the case where the mode mismatch exist and there are contributions from two-mode-squeezing, the ratio of single photon component, two photons component and three photons component become approximately 85%, 1.9%, and 13.1%, respectively. The 1.9% two photons component is incoherent with single and three photons component because there exist photon in an orthogonal mode when partial trace is taken. This two photons component causes the value of the origin of the Wigner function to increase by approximately 0.012. This impurity can be suppressed by using narrowband filitering cavity. Exact quantification of the impurities for the higher squeezing level and the multiphoton subtraction requires further study. But the impurity should increase as the squeezing level increases because the contribution of multiphoton components become more. Despite the fact that the impurity seems small, this impurity is important as we pursue the generation of an ideal cat states for CV quantum computation. Also, in the generation of cat state with large amplitude, this impurity will become more apparent, thus it is important to suppress this impurity.

To efficiently utilize cat states in MBQC, in addition to the purity, the shape of the temporal mode and the ability to obtain the quadrature value in real time is also equally important. In MBQC, the input states are entangled with a resource state called cluster state, and the operations are carried out by a measurement on each mode of the cluster state. When the modes are measured, the measurement results need to be fed forward to the next step of the operations. Linear feed-forward operations for each measurement can be postponed and performed after all measurements have finished [24]. On the other hand, non-linear feed-forward operations cannot be postponed and have to be done before the next operation step. This means that the acquisitions of the quadrature values must be performed in real time in order to realize efficient non-linear feed-forward operations. Therefore, real-time quadrature measurement is an important piece in the universal MBQC since such non-linear feed-forward operations are necessary for a non-Gaussian operation [25], which will allow us to perform quantum information processing that surpass classical computation [26, 27].

Optics EXPRESS

Real-time quadrature measurement of single photon states has already been demonstrated by generating single photon states with an exponentially rising temporal mode [28]. In their method, non-degenerated and asymmetric OPO is used for the temporal mode shaping. Therefore, their method is not applicable to quantum states that needed a degenerated OPO in the generation, such as cat states. Another method of the temporal mode shaping using optical cavities has already succeeded in the case of single photon states [29, 30]. However, there has not been any demonstration of the temporal mode shaping of the quantum states with multiple photons or with phase information.

In this paper, we use a narrowband filtering cavity in the subtracted photon path to limit the frequencies of the subtracted photons to where the squeezing level is almost constant (Fig. 1(c)). This method has two main advantages over the previous method. First, in principle, we can generate pure cat state, which is theoretically impossible with previous photon subtraction [23]. Even though filtering cavities are already used for filtering out non-degenerated photon pairs in the previous demonstration of cat states [15, 16], the frequency bandwidth of the filtering cavity is much wider than that of the OPO, so that raw photon correlation of OPO can be utilized. Second, the temporal mode of the cat states generated by this method becomes exponentially rising mode, which we utilize to perform real-time quadrature measurements. This is because the spectral filtering of subtracted photons is equivalent to the temporal mode shaping of the cat states. Therefore, the temporal mode becomes exponentially rising due to the frequency response of the narrowband filtering cavity in our method, while the temporal mode is double-sided exponential in the previous method due to the time correlation function of the OPO. The establishment of the highly pure generation method, combining with the real-time quadrature measurement of cat states, will facilitate the usage of the cat states in MBQC, thus expanding the potential of MBQC.

2. Experimental setup

We used a broadband OPO and a narrowband filtering cavity to demonstrate the generation of highly pure cat states by optical filtering (Fig. 1(c)). In [31], cat state was generated with an OPO with bandwidth of approximately 10 MHz. Therefore, in order to demonstrate photon subtraction with narrow bandwidth using the OPO with the same specification, we have to use a filtering cavity which has much narrower bandwidth (for example, 1 MHz) . In that case, the generation rate will drop drastically which is not favorable experimentally, and the effect of low frequency noises such as laser noise might also become more apparent. To avoid these problems, we made a broadband OPO and made a filtering cavity whose bandwidth is narrow compare to this OPO (Fig. 1(c)).

The schematic diagram of the experiment setup is shown in Fig. 2. A CW Ti:Sapphire laser (M-squared, Sols:TiS) whose wavelength is 860 nm is used as a light source for this experiment. A 430 nm CW pump beam for the OPO is produced from a bow-tie shaped second harmonic generator. A rectangular shaped reference cavity (not shown in Fig. 2) between the second harmonic generator and the OPO is provided for matching the transversal modes of the pump beam and the OPO. The OPO used in this experiment is a triangle-shaped cavity with the same design as in [32] with the linewidth of 65 MHz, and a 10 mm long periodically poled $KTiOPO_4$ (PPKTP) crystal is placed inside the OPO and used as a nonlinear medium.

A beamsplitter with reflectivity of $R = 0.97$ is used for tapping a single photon from squeezed vacuum. There are three filtering cavities (FC-1, FC-2, FC-3) on the subtracted photon path. FC-1 and FC-3 are Fabry-Pèrot cavities with large free spectral range (FSR) and acts as frequency filters that filter out unwanted non-degenerated photon pairs. On the other hand, FC-2 is a triangle-shaped narrowband cavity with half-width half-maximum (f_{HWHM}) much narrower than the OPO. This cavity is used to limit the frequency bandwidth of the subtracted photons. The detailed parameters of all the filtering cavities are shown in Table 1. We put an isolator between FC-1 and FC-2 to prevent coupling between FC-1, FC-2 and FC-3. We also put another isolator

Optics EXPRESS

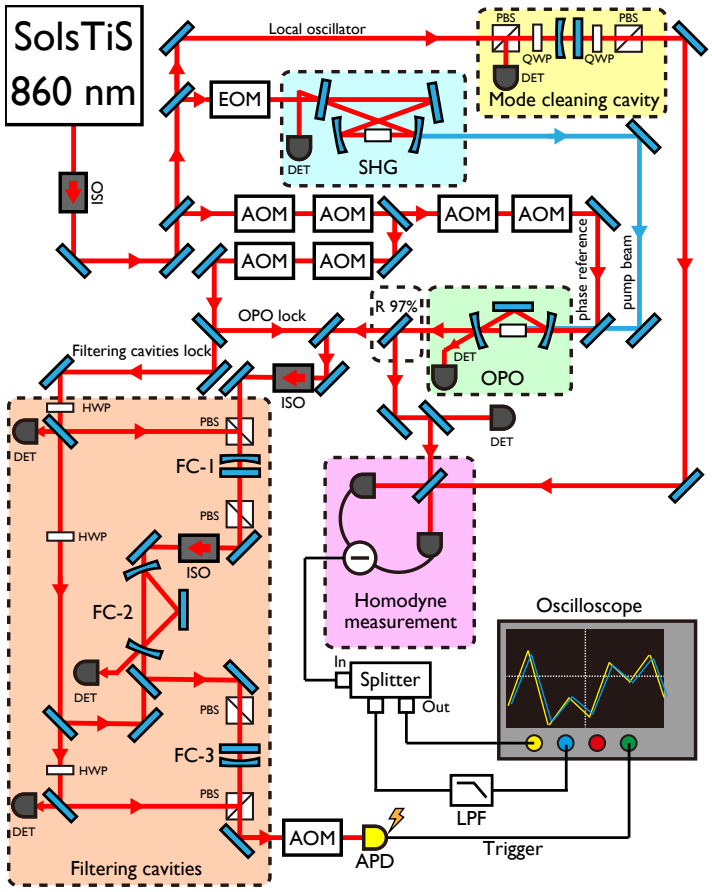

Fig. 2. Schematic diagram of the experiment setup. Only important optical components are included in the figure. Piezoelectric components and electrical channels for feedback and control are omitted. Red lines denote 860 nm laser beam, while blue lines denote 430 nm laser beam. SHG: Second harmonic generator. ISO: Isolator. HWP: Half-wave plate. QWP: Quarter-wave plate. PBS: Polarization beamsplitter. EOM: Electro-optic modulator. AOM: Acousto-optic modulator. APD: Avalanche photodiode. FC: Filtering cavity. LPF: Low-pass filter. DET: Detector. Detectors shown in the figure are for detecting error signal used in cavities locking and such.

Table 1. Parameters of the OPO and filtering cavities

	Shape	Length (mm)	Reflectivity	FSR (GHz)	f_{HWHM} (MHz)
OPO	Triangle	46.3	HR, HR, 0.86	5.32	65
FC-1	Fabry-Pèrot	1.99	0.994, 0.994	75.4	68
FC-2	Triangle	103	0.98, HR, 0.98	2.91	9.4
FC-3	Fabry-Pèrot	2.89	0.994, 0.994	51.9	47

between the OPO and FC-1 to prevent lock beams of filtering cavities from reaching the OPO. Note that it is possible to use two cavities where one of the cavities has high finesse, thus narrow bandwidth, instead of using three cavities. This alternative requires less number of cavities, but high finesse cavity is more difficult to make and control.

To characterize the generated states, we performed homodyne measurements. The homodyne

Optics EXPRESS

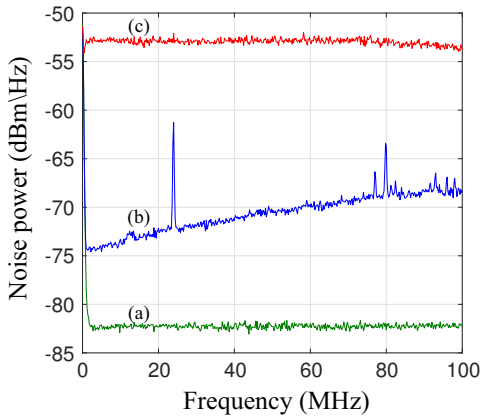

Fig. 3. Characteristic of homodyne detector measured with spectrum analyzer. (a) Noise of spectrum analyzer. (b) Circuit noise. (c) Shot noise. LO power is 20 mW. The data here are taken with resolution bandwidth of 200 kHz, and averaged over 300 sweeps.

detector used here has a wide bandwidth of approximately 100 MHz with photodiodes that have the quantum efficiency higher than 98% [32]. The characteristic of the homodyne detector used in this experiment is shown in Fig. 3. Matching transversal modes between a local oscillator (LO) and measured beams is important in homodyne detection. To do so, we put the LO beam through a mode cleaning cavity which filters the transversal mode of the LO into TEM_{00} and resulted in interferometric visibility of 99% in homodyne measurement.

A phase reference beam is introduced into the OPO for locking the phase between the generated states and the LO at homodyne detector. We used two acousto-optic modulators (AOM) to shift the frequency of the phase reference beam by +100 kHz for phase locking. When the phase reference beam goes through the OPO, due to difference frequency generation (DFG), the electric fields of frequency ±100 kHz relative to the carrier frequency will be generated. The resultant electric field vector will elliptically oscillate in the complex plane of the frame rotating with the carrier frequency, while the electric field will circularly rotate in the case of detuning without DFG. If we look at the intensity of the phase reference beam, the intensity oscillates at 200 kHz. By demodulating this intensity, we can lock the relative phase between phase reference beam and pump beam. Moreover, when the phase reference beam and the LO interfere, the resultant intensity will oscillate with frequency of 100 kHz. We can lock the phase between the phase reference beam and the LO by properly demodulating the interference signal. This demodulation is not so trivial because the complex amplitude of phase reference beam is elliptic due to DFG. By locking the relative phase between the phase reference beam and the LO and between the phase reference beam and the pump beam, we indirectly lock the relative phase between a cat state and the LO. Since we are locking relative phases by using demodulation of the beat signals, we can lock at any arbitrary relative phase by changing the phase of the demodulation signal. This locking method using phase reference beam with DFG gives error signal with better S/N ratio than the usual method using phase modulation because the size of the error signal is proportional to the strength of the carrier not the strength of the phase modulation.

We used Pound-Drever-Hall technique [33] for locking the second harmonic generator. An electro-optic modulator (EOM) is put in front of the second harmonic generator for generation of the error signal. For the OPO and filtering cavities, we used tilt locking technique [34]. We also shifted the frequency of the cavity lock beams by 200 kHz to prevent unwanted interference with other beams.

Optics EXPRESS

In this experiment, the phase reference beam and cavity lock beams (collectively called control beams) are turned on and off periodically by AOMs. Beside two AOMs in the path of phase reference beam and cavity lock beams, there are two more AOMs that are common to both beams in order to increase the extinction rate of the control beams. All the aforementioned cavity locking and phase locking is performed by electrical feedback using servo amplifiers when the control beams are turned on. When the control beams are turned off, the optical system is held in the same state before the control beams are turned off. Using this periodic switching, we prevented the control beams from reaching the APD, which will result in fake clicks that degrade the purity of the cat states.

3. Experimental results

For the rest of the paper, we refer to the measurement where we digitally integrate the electric signal with the temporal mode as post processing, as opposed to real-time measurement where the electric signal is continuously integrated with the temporal mode by a low-pass filter (LPF) [28].

In this paper, we performed photon subtraction from squeezed vacua with three different squeezing level. To characterize each state, we performed homodyne measurements for 37 phases from 0 degrees to 180 degrees with 5 degree step and we collected data of 10,000 events for each phase. The electric signal from a homodyne detector is split into two paths and we put a LPF for real-time measurement in one of the paths and simultaneously record unfiltered and filtered electric signal using an oscilloscope. To extract the quadrature values from CW homodyne measurement, we need to integrate the electric signals from homodyne detector with the temporal mode [35]. Also, in order to design and make a LPF for real-time measurement, we need to know the shape of the temporal mode of cat states beforehand. This means that it is important that we estimate the temporal mode correctly. Using the obtained quadrature values, we estimate the density matrices and the Wigner functions for both measurements using maximum likelihood method [36, 37].

In this section, we show the experimental results in the following order. First, we show the estimation of the temporal mode of the generated states. Then, we show the Wigner functions estimated from the quadrature values which are obtained by using the estimated temporal mode. We can evaluate the quality of the states generated via photon subtraction by the value at the origin of the Wigner functions, which we call Wigner negativity. In the ideal case, the Wigner negativity is $W(0,0) = -1/\pi \approx -0.318$ which is due to the fact that the states generated by subtracting a single photon from squeezed vacua have only odd photon numbers [12]. We also evaluate whether the effects of the experimental imperfections are consistent with the estimated Wigner functions. Finally, to verify the success of the real-time measurement, we show the correlation plot between the quadrature values of post processing and real-time measurement. As a qualitative indicator, we also show the screen capture of oscilloscope recording the electric signals from homodyne detector.

First, let us look at the temporal mode of the generated states. The temporal mode of the states generated by photon subtraction depends on the time correlation function of the OPO and the response function of filtering cavities. For the OPO, the time correlation function localized around time t_0 when the pump power is low, which holds in our experiment, has the following form [38]

$$g_{\mathrm{OPO}}(t;t_0) = \sqrt{2\pi f_{\mathrm{HWHM}}}\exp(-2\pi f_{\mathrm{HWHM}}|t-t_0|). \tag{1}$$

For filtering cavities, the response function is equivalent to an ideal Lorentzian filter and can be expressed in time domain as follows [38]

$$g_{\mathrm{filter}}(t;t_0) = \sqrt{4\pi f_{\mathrm{HWHM}}}\exp(-2\pi f_{\mathrm{HWHM}}|t-t_0|)\Theta(t_0-t), \tag{2}$$

where $\Theta(t)$ is Heaviside step function.

Optics EXPRESS

In our case, we have three filtering cavities. Therefore, the temporal mode of the generated states will become a time convolution between the time correlation function of the OPO in expressed by Eq. (1) and the response function of three filtering cavities expressed by Eq. (2) with f_{HWHM} which corresponds to parameter of each cavity (Table 1). After performing time convolution, the ideal temporal mode $g_{\mathrm{ideal}}(t;t_0)$ can be expressed as follows

$$g_{\mathrm{ideal}}(t;t_0) = N\left[\sum_{i=1}^{4} c_i \exp(-2\pi f_i|t-t_0|)\Theta(t_0-t) + \left(\sum_{i=1}^{4} c_i\right)\exp(-2\pi f_i|t-t_0|)\Theta(t-t_0)\right], \tag{3}$$

where N is a normalization constant, i =1–3 corresponds to filtering cavities, $i = 4$ corresponds to the OPO, and f_i corresponds to bandwidth of each cavity. $c_1 = 2f_4(f_3 - f_2)/f_4^2 - f_1^2)$ and c_2, and c_3 are the cyclic permutation. The expression for c_4 and N are

$$c_4 = \frac{f_1 - f_2}{f_4 - f_3} + \frac{f_2 - f_3}{f_4 - f_1} + \frac{f_3 - f_1}{f_4 - f_2}, \tag{4}$$

$$N = \frac{1}{\sqrt{2\pi}}\left[\sum_{i,j=1}^{4} \frac{c_i c_j}{f_i + f_j} + \frac{1}{2f_4}\left(\sum_{i=1}^{4} c_i\right)^2\right]^{-\frac{1}{2}}. \tag{5}$$

From Eq. (3), we can see that when one of the f_i of the filtering cavities is much smaller than that of the OPO and all the other cavities, which corresponds to the case where there is a narrowband filtering cavity, that term becomes dominant and $g_{\mathrm{ideal}}(t;t_0)$ approaches exponentially rising temporal mode. The mode mismatch of the temporal mode from exponentially rising mode can be made arbitrary small by making the filter cavity narrower. Also, if the bandwidth of the filter cavity is much narrower than that of the OPO, the effect of the pump power on the time correlation function of OPO, thus on the temporal mode of the generated states, is negligible because the effect of narrowband filtering cavity is dominant. This means that another merit of narrowband filtering cavity is that the temporal mode is almost unchanged by the pump power. This property might be useful when considering generation of quantum states using photon subtraction from highly squeezed vacua.

We used independent component analysis (ICA) [39], where the non-Gaussianity induced via photon subtraction is utilized, to find a set of independent modes and estimate the temporal modes of the generated states. We measured the quadrature for the phase that corresponds to largest variance and used the quadrature data of 10,000 events at that phase in the temporal mode estimations. Another method similar to ICA is the estimation via principal component analysis (PCA) [40, 41], which make use of the fact that the variances of the heralded states are larger than the initial squeezed vacua.

The temporal mode of the cat state is shown in Fig. 4. The solid curve is the estimated temporal mode and the dashed curve is the theoretical prediction from the experimental parameters using Eq. (3). The inner product between these two curves is 0.996 . The dotted curve is the temporal response of the 3rd-order LPF that is designed for real-time measurement. The design of the LPF is shown in Fig. 5. We optimize the parameters of the LPF so that the inner product between the response function of the LPF and the estimated temporal mode is the highest. The parameters of the LPF here are for the case where the output impedance of the homodyne detector Z_{hom} and the input impedance of the oscilloscope Z_{osc} are 50 Ω. The inner product of the response of this LPF to the estimated temporal mode is approximately 0.988. From these results, it is clear that the temporal mode of the generated states is consistent with the theoretical prediction and the designed LPF is also consistent with the temporal mode of the generated states. We integrated the electric signal from homodyne detector with this estimated temporal mode to obtain the quadrature values for post processing. For real-time measurements, we used the LPF

Optics EXPRESS

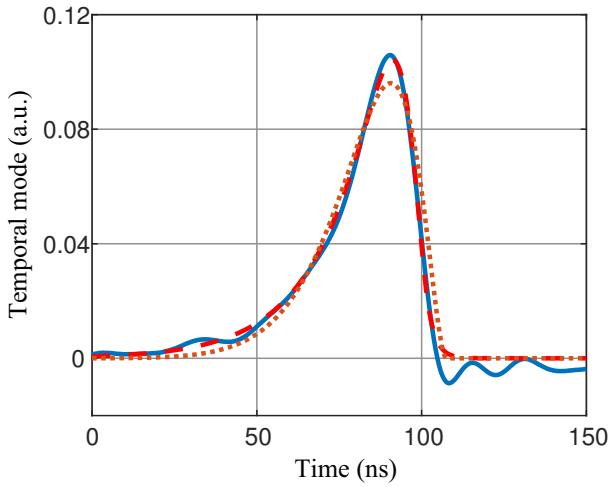

Fig. 4. Temporal modes of generated cat state. Solid curve: estimated temporal mode. Dashed curve: Theoretical prediction from experiment parameters. Dotted curve: Temporal response of low-pass filter used in real-time measurement.

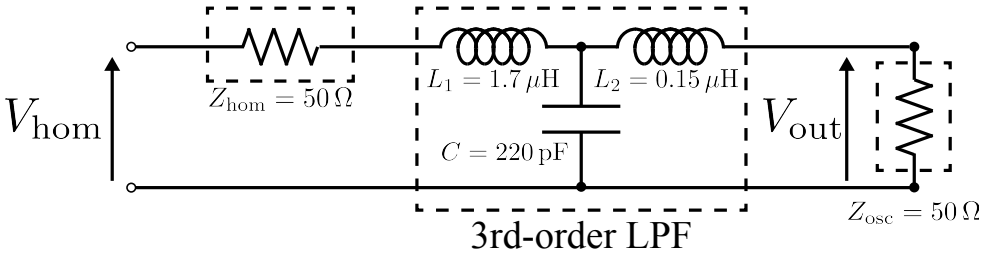

Fig. 5. 3rd-order LPF designed for real-time measurement. V_{hom}: Electric signal from homodyne detector. Z_{hom}: Output impedance of homodyne detector. Z_{osc}: Input impedance of oscilloscope. V_{out}: Output signal measured at oscilloscope.

to continuously integrate the electric signal in real-time measurement, and we pick the value of electric signal from oscilloscope trace at the timing which corresponds to generation of cat state. This timing can be found by looking at the variance of the electric signal recorded with real-time measurements; The variances is the largest when the integration with LPF picks out only cat states. The timing depends on both optical and electrical delay and is needed to be characterized only once for a given setup.

Figure 6 shows the squeezing spectra of the initial squeezed vacua used for generation of the states. The squeezing spectra are described by the following equation [38];

$$S_{\pm}(f) = 1 \pm (1 - L)\frac{4\xi}{(1 \mp \xi)^2 + (f/f_{\mathrm{HWHM}})^2}, \tag{6}$$

where $\xi = \sqrt{\frac{P}{P_{\mathrm{th}}}}$ is the normalized pump amplitude. P and P_{th} are the pump power and the threshold pump power of the OPO, respectively. The threshold pump power of the OPO used in this experiment is approximately 400 mW. L is the total external loss, and f_{HWHM} is the bandwidth of the OPO. In this experiment, we used the squeezed vacua with ξ =0.11, 0.25, 0.39 for generation of quantum states. The losses in this experiment are as follows: 1.2% propagation loss, 2% loss due to quantum efficiency of photodiodes, 1% loss due to circuit noise of the

Optics EXPRESS

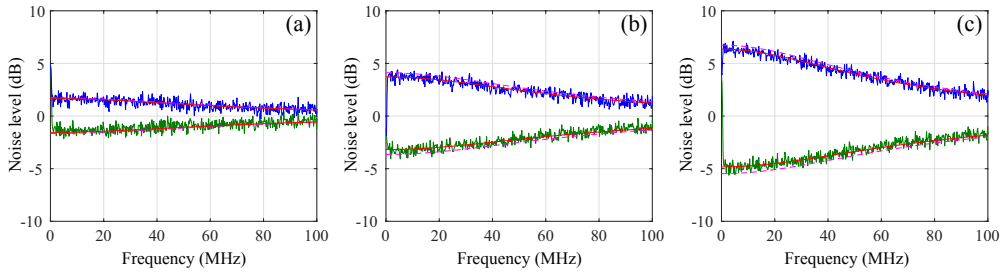

Fig. 6. Squeezing spectra of the initial squeezed vacua normalized to vacuum. (a) $\xi = 0.11$, (b) $\xi = 0.25$, and (c) $\xi = 0.39$. Dashed pink lines: theoretical plots of squeezing spectra using Eq. (6) where the external loss for all cases are $L = 0.113$. Solid red lines: fitting of Eq. (6) to squeezing spectral with $L = 0.162$. Note that both L included 3% loss due to $R = 0.97$ beamsplitter used in photon subtraction.

homodyne detector, 2% loss due to visibility at homodyne measurement, and 2.1% loss due to the escape efficiency of the OPO. Therefore, the total experimental loss in this experiment is 8.3%. In the measurement of the squeezing spectra there is an extra 3% loss due to $R = 0.97$ used in photon subtraction. Note, however, that we ignored the frequency dependence of the circuit noise of the homodyne detector. This is because the cat states generated in this experiment has bandwidth of approximately 10 MHz, which is much narrower than the bandwidth of the homodyne detector. The theoretical plots of the squeezed spectral are shown with dashed pink lines in Fig. 6. The difference between the measurement results and the theoretical predictions might come from parameters we could not directly or accurately measure such as quantum efficiency of photodiodes. To obtain more accurate approximation of the total losses, we perform fitting to squeeze spectral and the results are shown with solid red lines in Fig. 6. From the fitting results, the total loss is approximately 16%, which equivalent to 13% loss in photon subtraction.

Figure 7 shows the Wigner functions and the photon number probability distributions for post processing and corresponding real-time measurements.

Figure 7(a) shows the post processing measurement results of photon subtraction from squeezed vacua with $\xi = 0.11$, which corresponds to the pump power of 5 mW and the initial squeezing level of 1.0 dB near DC component. The generation rate of this state is about 1,200 counts per second (cps). The ratio of single photon in the generated state is 0.74, and the Wigner negativity is -0.176 ± 0.001. The uncertainties of the Wigner negativities are calculated by using bootstrapping method [42]. We can see from the Wigner function that this state is slightly squeezed. This means that despite the fact that the generated state consists of mostly single photon component, the generated state is not single photon state and this slight squeezing is due to the initial squeezing level. If we lower the squeezing level even more, the generated state will be less squeezed, but the generation rate will become lower, and the effect of fake counts will become more apparent.

Figure 7(b) shows the post processing measurement results of photon subtraction from squeezed vacua with $\xi = 0.25$, which corresponds to the pump power of 25 mW and the initial squeezing level of 3.0 dB near DC component for generation of quantum state with high fidelity to a minus Schrödinger's cat state $|\Psi_{\text{cat},-}(\alpha)\rangle \propto |\alpha\rangle - |-\alpha\rangle$ with $|\alpha|^2 = 1$ [13]. The generation rate of this state is about 4,800 cps. The Wigner negativity of the generated cat state is -0.184 ± 0.001 without loss corrections, which is the highest value ever observed without loss correction, compared to the previous record of -0.171 ± 0.003 [31]. The fidelity F to the cat state is calculated by $F = \langle \Psi_{\text{cat},-}(\alpha)|\hat{\rho}|\Psi_{\text{cat},-}(\alpha)\rangle$, where $\hat{\rho}$ is the density matrix of our state. The resulting fidelity is $F = 0.782$ to a Schrödinger's cat state with $|\alpha|^2 = 1.02$, which is also the highest value ever observed without loss correction.

Optics EXPRESS

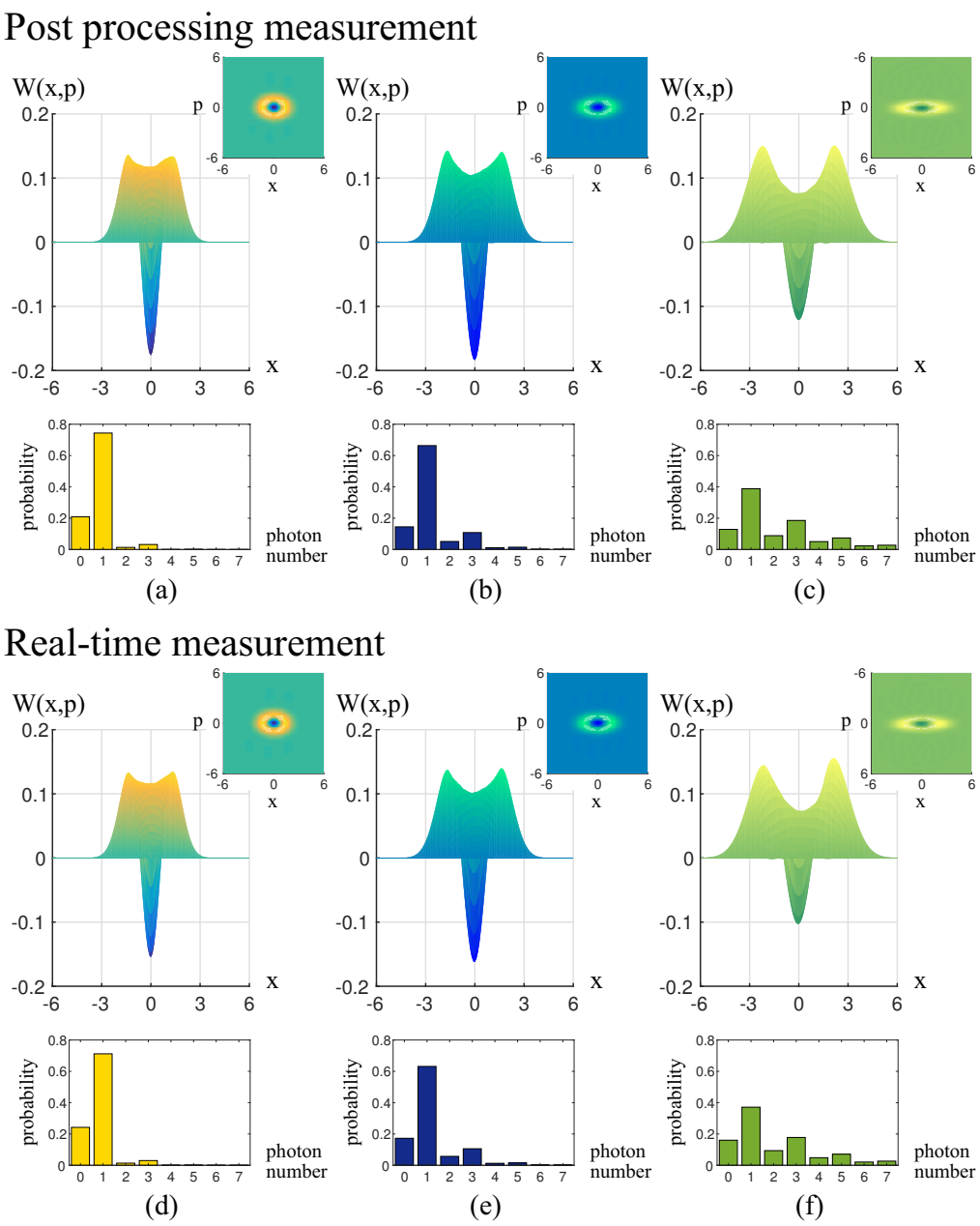

Fig. 7. Wigner functions and photon number probability distributions of states generated in this experiment. The upper-half is the results of post processing measurement, while the lower half is the corresponding real-time measurement. (a,d) $\xi = 0.11$. (b,e) $\xi = 0.25$. (c,f) $\xi = 0.39$. For post processing measurements, Wigner negativities are -0.176 ± 0.001, -0.184 ± 0.001, and -0.121 ± 0.002 respectively. For real-time measurement, Wigner negativities are -0.154 ± 0.001, -0.162 ± 0.001, and -0.102 ± 0.001 respectively. The initial squeezing spectra are shown in Fig. 6.

Figure 7(c) shows the post processing measurement results of photon subtraction from squeezed vacua with $\xi = 0.39$, which corresponds to the pump power of 60 mW and the initial squeezing

Optics EXPRESS

Table 2. Mixedness due to the imperfection in the photon subtraction

	Quantum states		
	$\xi = 0.11$	$\xi = 0.25$	$\xi = 0.39$
Fake counts	2.7%	0.7%	0.2%
Two photons subtraction	1.7%	2.7%	4.8%

level of 5.0 dB near DC component. The generation rate is about 16,000 cps. The Wigner negativity is -0.121 ± 0.002, which means that this state also possess high nonclassicality. The degradation of the Wigner negativity of this state with $\xi = 0.39$ is more than that of states with $\xi = 0.11, 0.25$. This is due to the fact that the state with $\xi = 0.39$ has more mean photon number than the other two states. In [16], the photon subtraction from the initial squeezing level of 3.7 dB was performed as a demonstration of photon subtraction from highly squeezed vacua. In that experiment, the four photon probability is larger than five photon probability. On the other hand, even with large squeezing, the odd photon probabilities are larger than the adjacent even photon probabilities in our experiment, and we can observe large photon number components clearly. We believe that this is the effect of narrowband filtering [23], which becomes more apparent as the initial squeezing level increase.

In addition to losses, the generated states are degraded due to fake counts of the APD and the probability of subtracting two photons instead of one. Fake counts cause the generated states to become mixed with the initial squeezed vacua, while subtracting two photons caused the states to become mixed with two photons subtracted states. These sources of degradation are different from the degradation due to losses which corresponds to the contamination of vacua, and we will refer to this type of degradation as mixedness. The mixedness due to fake counts can be measured directly, and the probability of two photon subtraction can be estimated using the normalized pump amplitude ξ and the reflectivity of beamsplitter R used in photon subtraction [12], where we ignore the probability of subtracting more than two photons. The mixednesses in this experiment are shown in Table 2.

To see whether the generated states are consistent with experimental losses and mixedness, we perform the following calculation. First, from experimental parameters such as normalized pump amplitude ξ and reflectivity of beamsplitter R, we can calculate the density matrices for the generated states in the ideal case where there are no losses and mixnesses. Then, by applying losses and mixedness to the ideal states, we can simulate the states that would be generated by this experiment system. By comparing the Wigner negativity between the measured states and the simulated states, we can evaluate the consistency between the generated states are consistent with experimental parameters and imperfections. Performing the calculations, the Wigner negativity of the simulated three quantum states are -0.203, -0.182, and -0.135, respectively. Comparing this with the experimental Wigner negativities: -0.176 ± 0.001, -0.184 ± 0.001, and -0.121 ± 0.002, we can see that the Wigner negativities estimated from experimental parameters are consistent with the estimated results and the deviations are at most about 10%. Note that we treat the states as if they are single-mode-squeezed single photons in this calculation. This is possible in our experiment because the states generated here are single-mode in theory, unlike the previous photon subtractions.

Figures 7(d), 7(e), and 7(f) show the results of real-time measurement in the case of ξ =0.11, 0.25, and 0.39, respectively. Qualitatively, the Wigner functions is in good agreement with results of post processing. The Wigner negativity of each state is -0.154 ± 0.001, -0.162 ± 0.001, and -0.102 ± 0.001, respectively. Although the Wigner negativity of real-time measurement is still high, it is smaller than the corresponding post processing results. The difference in the Wigner negativities, which are approximately -0.02, are the same for all states. This indicates that the degradation of the Wigner negativities should be caused by common sources. When the electric

Optics EXPRESS

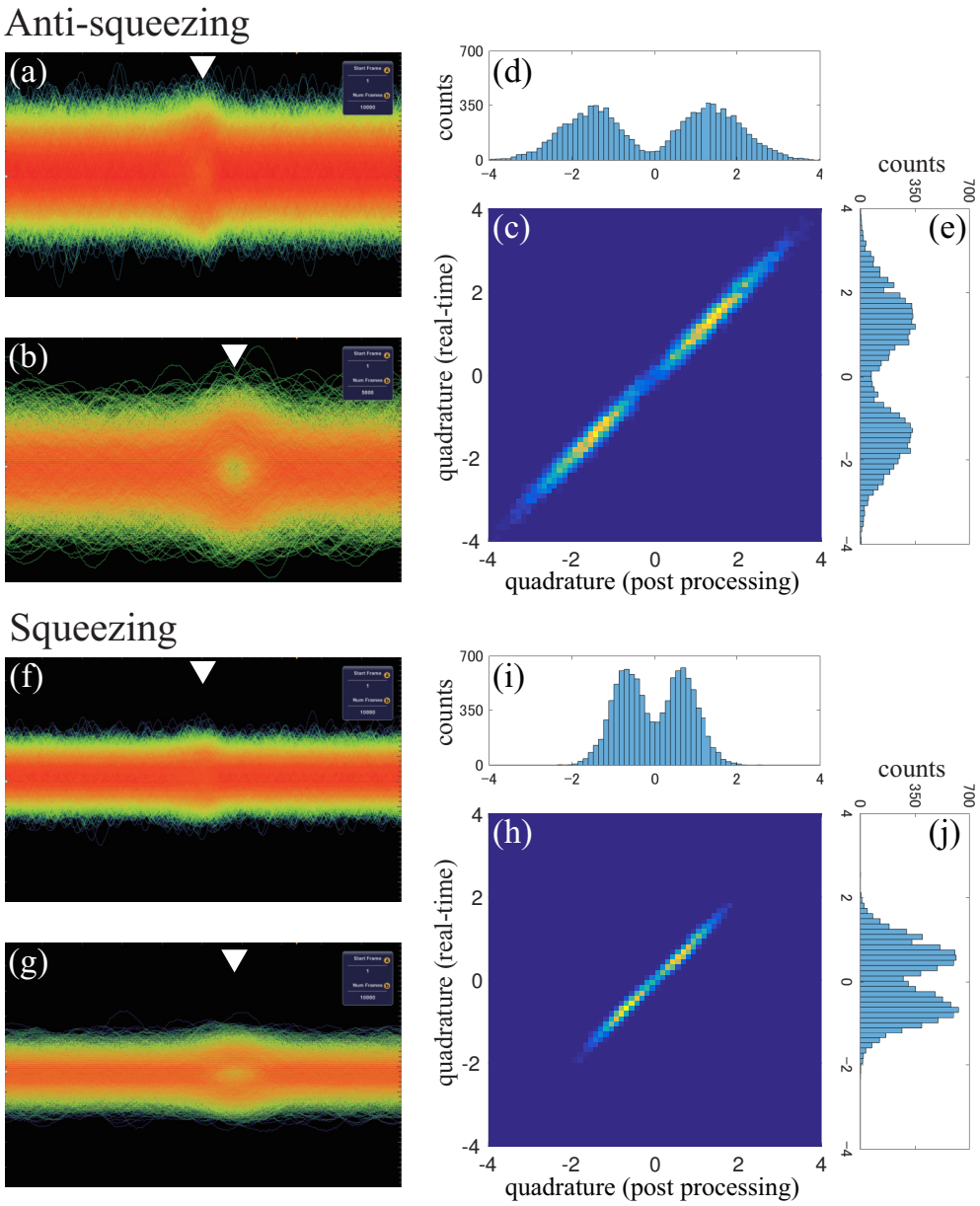

Fig. 8. Screen captures of oscilloscope displaying electric signal from homodyne detector and quadrature distribution of cat state of phases corresponded to anti-squeezing and squeezing. The number of the overlaid events is 10,000 and electric signal is recorded 200 ns around the timing of photon detection. For anti-squeezing: (a) Screen capture of post processing measurement. (b) Screen capture of real-time measurement. White triangle marks represent the timing of the generation of cat states ($\xi = 0.25$). The coloring represents frequency of the distribution at each time and change from blue to green, yellow and red as the frequency increase. (c) Correlation plot between quadrature of post processing and real-time measurement. (d) Quadrature distribution of post processing. (e) Quadrature distribution of real-time measurement (This corresponds to the histogram of electric signal at the white triangle mark in (b)) . The correspoding figures for squeezing are (f-j). (See Visualization 1 for the screen captures of real-time measurement for phases in between.)

Optics EXPRESS

signal from the homodyne detector is integrated with the mode that is not perfectly matched to the temporal mode of the generated state, the unmatched portion will pick up the squeezed vacuum instead of the state generated from photon subtraction. If the inner product between the mode defined by LPF and the temporal mode of the generated states is M, the modes mismatch becomes $1 - M^2$. The mode mismatch in this experiment is estimated to be $1 - M^2 = 1 - 0.988^2 = 2.4\%$. This extra mixedness in real-time measurements increase the Wigner negativity by 0.015 from post-processing results. Thus, the difference in the Wigner negativities can be explained by this mode mismatch.

As mentioned before, we can qualitatively verify the success of the real-time measurement by using the screen capture of the oscilloscope, and quantitatively by correlation plots of the quadrature values between the post processing and the real-time measurements. Figures 8(a) and 8(b) show the screen captures of the oscilloscope for the post-processing and real-time measurements of the cat state ($\xi = 0.25$) at the phase of anti-squeezing, and Fig. 8(f) and 8(g) show the corresponding at the phase of squeezing. In the case of the post processing, the histogram of electrical signal does not possess the characteristics of the cat state at any arbitrary timing. In the case of the real-time measurement, if we look at the electric signal at the timing corresponding to the generation of the cat states (at the triangle mark), the histogram of the electric signals possess the characteristics of quadrature distribution of cat states; a dip around quadrature equals to 0 and two peaks, and the variance for anti-squeezing and squeezing are different. For the other phases, we also got the histogram of the electric signals which possess the characteristics of the cat state at the same timing (See Visualization 1). This is the qualitative indicator that we succeeded in the real-time quadrature measurement. In addition, the screen captures of the oscilloscope are symmetric with respect to the generation timing in real-time measurement. When the temporal mode of the generated state and the mode defined by LPF are the same, the inner product between these two modes are the same for the same time difference, regardless of which comes first. Therefore, this symmetry is another qualitative indicator of the success of real-time measurement [28].

If the real-time measurement is successfully performed, the quadrature values obtained by real-time measurement and post processing measurement will have same values. Figures 8(c) and 8(h) shows the correlation between the quadrature of post processing and real-time measurements at the phase corresponded to anti-squeezing and squeezing, respectively. Figures 8(d), 8(i), 8(e), and 8(j) show the quadrature distribution of post-processing and real-time measurements, respectively. From Figs. 8(c) and 8(h), we can see that the quadrature values of both measurements are highly correlated for both anti-squeezing and squeezing. The correlation plots for all the other phases also show the similar correlations. The correlation coefficient r is defined by

$$r = \frac{\langle (x_{\text{real}} - \langle x_{\text{real}} \rangle)(x_{\text{post}} - \langle x_{\text{post}} \rangle) \rangle}{\sqrt{\langle (x_{\text{real}} - \langle x_{\text{real}} \rangle)^2 \rangle \langle (x_{\text{post}} - \langle x_{\text{post}} \rangle)^2 \rangle}}, \tag{7}$$

where x_{real} and x_{post} are quadrature values for real time and post-processing measurements, and $\langle \cdot \rangle$ is the expectation value. The correlation coefficient between the quadrature values of post processing and real-time measurements are over 0.99 for all phases which indicates that the results for both measurements are highly correlated.

4. Conclusion

We generated highly pure Schrödinger's cat states with a new method via optical filtering. It has been shown that this method has no theoretical limit on the purity of generated states as opposed to the previous photon subtraction. We succeeded in the generation of Schrödinger's cat state that has a new Wigner negativity record of -0.184 ± 0.001 without any loss corrections. From another aspect, optical filtering can be considered as temporal mode shaping, and the temporal

Optics EXPRESS

mode becomes exponentially rising with our method, which allows us to demonstrate a real-time quadrature measurement. In the real-time measurement, the states we generated showed high nonclassicality and the quadrature values are highly correlated with that of the post processing. This indicates that we succeeded in the real-time measurement of cat states, which is the first real-time quadrature measurement of quantum states with multiple photons and phase sensitivity.

This method can be easily extended to any quantum states that can be generated by photon subtraction or heralding, and allows us to perform photon subtraction from highly squeezed vacua. Therefore, this method is the most promising and realistic in the generation of highly pure quantum states and, at the same time, temporal mode shaping for the applications in MBQC. We expect that photon subtraction with narrowband optical filtering will become a new basis for generation of even more complex highly pure nonclassical states, which will accelerate the development of CV optical quantum information processing.

Funding

CREST (JP- MJCR15N5) of Japan Science and Technology Agency (JST), KAKENHI of Japan Society for the Promotion of Science (JSPS), and APSA of Ministry of Education, Culture, Sports, Science and Technology of Japan (MEXT).